

DOI: 10.1002/

Article type: Full Paper

Self-Healing, Flexible, and Tailorable Triboelectric Nanogenerators for Self-Powered Sensors based on Thermal Effect of Infrared Radiation*Xingyi Dai¹, Long-Biao Huang^{2*}, Yuzhang Du¹, Jiancheng Han², Qiuqun Zheng², Jie Kong^{1*} and Jianhua Hao^{3*}*¹X. Dai, Dr. Y. Du, Prof. J. KongMOE Key Laboratory of Materials Physics and Chemistry in Extraordinary Conditions
Shaanxi Key Laboratory of Macromolecular Science and Technology, School of Science
Northwestern Polytechnical University, Xi'an, 710072, P. R. China

*Corresponding Author, E-mail: kongjie@nwpu.edu.cn

²Dr. L.-B. Huang, J. Han, Q. ZhengCollege of Physics and Optoelectronic Engineering
Shenzhen University, Shenzhen, 518060, P. R. China

*Corresponding Author, E-mail: huanglbh@hotmail.com

³Prof. J. Hao

Department of Applied Physics

The Hong Kong Polytechnic University, Hong Kong, P. R. China

*Corresponding Author, E-mail: jh.hao@polyu.edu.hk

Keywords: triboelectric nanogenerators, self-powered sensors, self-healing, infrared radiation, reversible bonds.

Abstract

1
2
3 Self-healing triboelectric nanogenerators (TENGs) with flexibility, robustness and
4 conformability are highly desirable for promising flexible and wearable devices, which can
5 serve as durable, stable and renewable power supply, as well as self-powered sensor. Herein,
6 we design an entirely self-healing, flexible and tailorable TENG as a wearable sensor to
7 monitor human motion, with infrared (IR) radiation from skin to promoting self-healing after
8 being broken based on thermal effect of IR radiation. Human skin is natural IR emitter,
9 providing favorable conditions for the device to function efficiently. The reversible imine
10 bonds and quadruple hydrogen bonding (UPy) moieties are introduced into polymer networks
11 to construct self-healable electrification layer. UPy-functionalized multi-walled carbon
12 nanotubes are further incorporated into healable polymer to obtain conductive nanocomposite.
13 Driven by the dynamic bonds, our designed and synthesized materials show excellent intrinsic
14 self-healing and shape-tailorable features. Moreover, there is robust interface bonding in the
15 TENG devices due to the similar healable networks between electrification layer and
16 electrode. The output electric performances of the self-healable TENG devices can almost
17 restore to their original state when the damage of the devices occurs. This work presents a
18 novel strategy for flexible devices, contributing to future sustainable energy and wearable
19 electronics.
20
21
22
23
24
25
26
27
28
29
30
31
32
33
34
35
36
37
38
39
40
41
42
43
44
45
46
47
48
49
50
51
52
53
54
55
56
57
58
59
60
61
62
63
64
65

1. Introduction

1
2 Self-powered devices, as an emerging field, which are capable of converting surrounding
3
4 energy into electrical energy, have shown great potential in various applications including
5
6 artificial skins, sensors, nanorobotics, and portable/wearable devices.^[1-5] Compared to the
7
8 electronic devices driven by conventional power sources such as batteries and capacitor with
9
10 the restrictions of bulky volume, limited lifetime and environmental unfriendliness, the self-
11
12 powered devices exhibit vast excellence. Recently, triboelectric nanogenerators (TENGs) as a
13
14 green and sustainable power source have derived great attentions due to their merits,
15
16 including wide material availability, diversified designability, low cost, and easy
17
18 fabrication.^[6-8] Based on the synergistic effect of contact electrification and electrostatic
19
20 induction between different triboelectric materials, TENGs could be effectively utilized to
21
22 harvest mechanical energy and generate electrical energy and signals.^[9-13]
23
24
25
26
27
28
29
30

31
32 Currently, a number of polymers have been used and play critical roles as friction and
33
34 supporting materials in TENGs^[14-16]. However, unpredicted damage or performance loss of
35
36 TENG devices could be induced by the interface friction between different materials and
37
38 frequent mechanical deformation such as device bending, compressing, stretching, and
39
40 twisting. Self-healing polymer as novel materials have presented a preferred strategy to solve
41
42 above problems.^[17-19] Self-healing polymers could be classified into intrinsic and extrinsic
43
44 kinds.^[20] Compared with extrinsic systems, intrinsically healable materials are usually flexible
45
46 and deformable.^[21-22] Therefore, intrinsic self-healing polymers induced by supramolecular
47
48 interaction^[23-24] or reversible covalent bonds^[25-27] could be ideal materials for self-healing
49
50 TENGs. The supramolecular systems are physically reversible based on noncovalent
51
52 interactions with rapidly exchanging.^[28-31] Moreover, reversible covalent bonds are relatively
53
54 stable and robust under ambient conditions, while adaptable under certain stimuli.^[32-35]
55
56
57
58
59
60
61
62
63
64
65

1 Recently, continuous efforts have been made to develop self-healing TENGs. Hao et al.
2 indicated a fully self-healing TENG with disulfide bonds in Polydimethylsiloxane-
3 polyurethane (PDMS-PU) and magnetic-assisted electrode.^[36] Wang et al. transferred the Ag
4 nanowires and poly(3,4-ethylenedioxythiophene) (Ag-PEDOT) film to imine-containing
5 PDMS to achieve a self-healable, stretchable, and transparent TENG as soft power sources.^[37]
6
7 Pan et al. prepared a near-infrared irradiation induced remote TENG through embedding
8 carbon nanotubes (CNTs) in self-healable elastomer and assembling with PDMS.^[38] Lai et al.
9 developed an entirely self-healable, highly transparent, and superstretchable TENGs by
10 encapsulating hydrogen bonding-based hydrogel within metal-ligand-based PDMS^[39]. Most
11 of the healable devices are dependent on magnetism, NIR, or even without external
12 stimulation. While the automatically self-healing system might be unstable or take longer time
13 to complete the self-healing process. Additionally, infrared (IR) radiation from human body is
14 ubiquitous but usually ignored in the use of daily life. Nevertheless, self-healing TENGs as
15 self-powered sensors with real-time repairing feature under skin thermal radiation are merely
16 reported.
17
18
19
20
21
22
23
24
25
26
27
28
29
30
31
32
33
34
35
36
37
38

39 In this work, taking advantage of heat converted from human IR radiation, an entirely self-
40 healing and soft TENG based on imine bond and UPy unit (IU-TENG) is prepared and
41 demonstrated as a self-powered sensor to detect human motion. Human skin could emit IR
42 light and radiate heat which can provide an ideal condition to promote self-healing action of
43 polymer. Both the triboelectric layer and electrode could be autonomously self-healable under
44 ambient environments, driven by the dynamic imine bond and quadruple hydrogen bonding
45 UPy motif. With the incorporation of UPy units into imine-based elastomers, the mechanical
46 performances of the materials could be significantly enhanced. The UPy-functionalized multi-
47 walled carbon nanotubes have been incorporated into the elastomer and form an electrode
48 with considerable conductivity. Meanwhile, for the devices of multilayered structures, the
49
50
51
52
53
54
55
56
57
58
59
60
61
62
63
64
65

1 robust interface bonding has been achieved, because each layer is based on the same healable
2 units. Moreover, the as-prepared IU-TENG device could present high electrical output
3 performances and self-healing as well as shape-tailorable features which could provide
4 promising possibility for the development and applications of TENGs.
5
6
7
8
9

10 11 **2. Results and Discussion**

12 **2.1. Design and Performance of Electrification Layer**

13
14 To fabricate the self-healing and robust TENG stimulated by thermal effect of IR radiation
15 from human body, the self-healable polymer matrix was designed and synthesized, as shown
16 in **Figure 1a**. The self-healing polymer-based networks were crosslinked by two kinds of
17 dynamic bonds (imine bond and UPy). Poly(propylene glycol) bis(2-aminopropyl ether) (PEA)
18 or bis(3-aminopropyl) terminated poly(dimethylsiloxane) (H₂N-PDMS-NH₂) was selected as
19 soft segment and it reacts with 2(6-isocyanatohexylaminocarbonylamino)-6-methyl-
20 4[1H]pyrimidinone (UPy-NCO) and 1, 1, 1-tris[(4-formylphenoxy)methyl]ethane (FPME) to
21 obtain flexible and healable polyazomethine (IU-PAM) and poly(dimethylsiloxane) (IU-
22 PDMS) elastomers based on imine and UPy units. **A catalytic amount of glacial acetic acid**
23 **was added to accelerate the reaction between amino and aldehyde groups to form imine bonds**
24 **(-CH=N-) in the synthesis process.** For IU-PAM, a signature peak at 8.23 ppm for imine
25 bonds, and the peaks at 10.13, 11.86 and 13.13 ppm assigned to the protons of UPy units
26 (Figure S2 of the Supporting Information) were obviously shown in the ¹H NMR spectra
27 (Figure S6 of the Supporting Information). Furthermore, a new peak at 1645 cm⁻¹ confirmed
28 the formation of -CH=N-, and the absence of the isocyanate bands at 2270 cm⁻¹ in the FTIR
29 spectra of Figure S7 (Supporting Information) revealed that isocyanate groups were
30 completely reacted and UPy moieties were grafted onto polymer chain. Similarly, the data of
31 IU-PDMS in Figure S8 and S9 (Supporting Information) indicated the successful synthesis. A
32 series of healable polyazomethine polymers (IU-PAM-0-3) with different molar ratio were
33
34
35
36
37
38
39
40
41
42
43
44
45
46
47
48
49
50
51
52
53
54
55
56
57
58
59
60
61
62
63
64
65

1 synthesized by varying amounts of UPy and imine moiety. The relative mechanical
2 properties were measured and shown in Figure 1b. With an increase in the contents of UPy,
3
4 the mechanical performances of polymers were significantly enhanced, which can be ascribed
5
6 to the rigid structure of UPy segments and the physical crosslinking between polymer chains
7
8 resulting from the UPy dimers. Served as noncovalent sacrificial bonds, the UPy dimers could
9
10 dissipate energy through reversible bond rupture during stretching. Meanwhile, the relatively
11
12 stronger imine bonds were able to maintain the network integrity.^[40-41] However, to a certain
13
14 extent, a mass of UPy can lead to lower flexibility of polymers. Therefore, IU-PAM-2 showed
15
16 the best mechanical properties with the fracture strain of 249% and maximum stress of 2.29 MPa,
17
18 which was selected to further investigate self-healing performances. Moreover, the ratio of
19
20 the reactants for IU-PDMS was designed according to that of IU-PAM-2.
21
22
23
24
25
26
27
28

29 The self-healing property was quantitatively investigated by uniaxial tensile tests. Dumbbell-
30
31 shaped specimens were bisected, and then recombined tightly under different healing
32
33 conditions. Figure 1c presents the typical stress-strain curve of IU-PAM-2 specimen before
34
35 and after healing from 6 to 12 h and then to 24 h. When the healing time was over 24 h, the
36
37 strain and strength of healed samples could restore to 244% and 2.23 MPa, respectively. For
38
39 IU-PDMS, as shown in Figure 1d, the healed specimens exhibited an elongation at breaking
40
41 point of 255 % and a tensile strength of 1.09 MPa after 24 h, which were almost coincident
42
43 with original specimens. The healing efficiency was found to enhance as healing time
44
45 extended. The healing efficiencies of both IU-PAM-2 and IU-PDMS specimens can reach
46
47 ~100% after being healed for 24 h, revealing that their mechanical performances could
48
49 completely revert to the original state and the polymers were provided with excellent self-
50
51 healing properties. Those results could be contributed to the critical role of the reversible
52
53 nature of imine bond and UPy motif.^[42-43] At the molecular level, the ‘mobile phase’ existing
54
55 on or near damaged area could promote intimate contact between scratched surfaces and
56
57
58
59
60
61
62
63
64
65

1
2
3
4
5
6
7
8
9
10
11
12
13
14
15
16
17
18
19
20
21
22
23
24
25
26
27
28
29
30
31
32
33
34
35
36
37
38
39
40
41
42
43
44
45
46
47
48
49
50
51
52
53
54
55
56
57
58
59
60
61
62
63
64
65

combine the reactive groups. Meanwhile, the low T_g of IU-PAM-2 (-58.9 °C) and IU-PDMS (-51.0 °C, Figure S10 of Supporting Information) enabled the polymer in a high elastic state and enhanced the movement of polymer chain at room temperature, which could facilitate self-healing. The active amino and aldehyde groups generated at the broken interface could reform imine bonds, accompanying with the imine exchange to achieve the integration of fracture surfaces. Moreover, the reformation of UPy dimers through the dissociated hydrogen-bonding could synergistically complete self-healing process.

2.2. Design and Performance of Electrode

The self-healable nanocomposite conductor was prepared by mixing ureidopyrimidinone functionalized multi-walled carbon nanotubes (MWCNTs-UPy) with IU-PAM-2, as illustrated in **Figure 2a**. The MWCNTs were functionalized with UPy units (Supporting Information for more details), and subsequently the nanoparticles were added to the solution of polymer containing UPy units (IU-PAM-2). The MWCNTs-UPy/IU-PAM nanocomposite film could be achieved with the evaporation of solvent. The UPy modified MWCNTs served as a part of physical cross-links, therefore quadruple hydrogen (UPy dimers) could be formed between particles and polymer chains,^[44] reinforcing the compatibility between the MWCNTs-UPy fillers and IU-PAM matrix. From the TEM image of MWCNTs-UPy/IU-PAM nanocomposite, it is seen that the nanoparticles are well dispersed in the matrix. The self-healable and conductive capabilities of MWCNTs-UPy/IU-PAM were investigated by connecting the as-prepared sample in a complete circuit composed of a light emitting diode (LED) bulb at first. As shown in Figure 2b, when the sample was cut into two parts, the lighted LED immediately went off. While the two pieces were tightly brought together and maintained at room temperature for 36 h, the LED bulb turned on again as that of the original intact MWCNTs-UPy/IU-PAM films, which indicated the good self-healing ability and electrical conductivity of the nanocomposite. Furthermore, IU-PDMS and MWCNTs-

1 UPy/IU-PAM nanocomposite samples were placed together with fully contact. As shown in
2 Figure 2c, the jointed sample exhibited a good elasticity and bonding strength under bending
3 and twisting, owing to the association-disassociation behaviors of imine bonds and UPy
4 dimers on the surface, which could extend the applications of as-prepared healable polymer
5 materials in flexible devices.
6
7
8
9
10

11
12
13
14 The tensile stress-strain curves of MWCNTs-UPy/IU-PAM for varying healing time at room
15 temperature were systematically researched and shown in Figure 2e. The pristine sample
16 showed a maximum strength of 2.13 MPa and breaking strain of 158%. The specimen healed
17 for 36 h recovered to about 2.12 MPa and 154%, respectively. The healing efficiency reached
18 up to 97%. In addition, it is known that CNTs have strong photothermal properties and they
19 are capable of absorbing near infrared (NIR).^[45-46] The self-healing abilities of MWCNTs-
20 UPy/IU-PAM were further investigated by using an intensity-modulated NIR solid-state diode
21 laser ($\lambda = 808$ nm). The images recorded by infrared camera in Figure 2d suggested that the
22 surface temperature rose rapidly upon NIR irradiation. A healing efficiency of 88% was
23 observed within 60 min for healing with NIR light exposure (Figure 2f), indicating that the
24 substantial photothermal effect promoted fast healing of wound areas. The electrical
25 conductivities were also quantitatively characterized, as shown in Figure 2g. Not only the
26 original one but also the healed samples with or without NIR irradiation exhibited favorable
27 conductive properties, which could further confirm the excellent self-healing performances of
28 MWCNTs-UPy/IU-PAM.
29
30
31
32
33
34
35
36
37
38
39
40
41
42
43
44
45
46
47
48
49
50
51
52

53 **2.3. Device Fabrication**

54
55
56 The fully self-healing IU-TENG device in single-electrode mode was successfully fabricated
57 by sandwiching the MWCNTs-UPy/IU-PAM nanocomposite film between the two IU-PDMS
58 films, as illustrated in **Figure 3a**. The IU-PDMS and MWCNTs-UPy/IU-PAM were regarded
59
60
61
62
63
64
65

1 as insulating layer and electrode, respectively. A copper tape was attached to the electrode
2 and extended out of the device for electrical connection. Most remarkably, there were robust
3 interface bonding in the IU-TENG device, ensuring the stability and robustness of the device
4 without delamination under frequently deformation. The interface bonding is exceedingly
5 important for the devices with multilayered structure. Without complex physical or chemical
6 post-processing, the good bonding interface was realized. Due to both of the electrode and
7 electrification layer containing dynamic imine bonds and UPy moieties, the different layers
8 could be seamlessly integrated into a single system through the exchange of dynamic bonds at
9 interfaces.
10
11
12
13
14
15
16
17
18
19
20
21
22
23

24 **2.4. Device Operation Principle**

25
26 The operation mechanism of the IU-TENG device is schematically described in Figure 3b,
27 originating from the comprehensive actions of contact electrification and electrostatic
28 induction. When two surfaces of the triboelectric materials (human skin and IU-PDMS) come
29 into contact, electrification could occur at the contact interface, leading to the generation of
30 electrostatic charges with opposite polarities. Owing to the IU-PDMS with higher surface
31 electron affinity compared to skin, the IU-PDMS could be negatively charged. Then, during
32 the separation of the charged surfaces, positive charges could be induced in the carbon
33 nanotubes to compensate static charges on the surface of IU-PDMS, and electrons flow from
34 MWCNTs-UPy to the ground, generating an instantaneous electrical current. Upon the
35 complete separation, the induced positive charges in the MWCNTs-UPy are equal to the
36 negative charges in the IU-PDMS, thus there is no potential difference. Once the skin is in
37 contact with IU-PDMS again, the electrons will flow in the opposite direction. By the
38 periodical contact-separation between the two triboelectric layers, an alternative current will
39 be continuously generated.
40
41
42
43
44
45
46
47
48
49
50
51
52
53
54
55
56
57
58
59
60
61
62
63
64
65

2.5. Device Performance

1
2 The electrical output performance of the IU-TENG with the size of 4 cm × 4 cm was
3 investigated and shown in Figure 3c-g. A commercial latex glove was utilized to perform
4 contact-separation motion with IU-TENG under a frequency of 3 Hz. The open-circuit voltage
5 (V_{oc}) could reach a maximum value of about 95 V. The peak short-circuit current (I_{sc}) and
6 transferred charge (Q_{sc}) were about 9.5 μ A and 43 nC, respectively. The output voltage and
7 current were resistance-dependent under different external loads. With the increment of
8 loading resistance, the output voltage increased and the current decreased. Correspondingly,
9 the maximum output power density was measured to be about 300 mW/m² when the load
10 resistance was 30 M Ω . As shown in Figure 3h, the IU-TENG was connect with thirty LEDs.
11 The green LEDs were all lighted up when the IU-TENG was pressed by human palm.
12
13
14
15
16
17
18
19
20
21
22
23
24
25
26
27
28

29 The IU-TENG has been demonstrated to exhibit good output electrical properties. During
30 practical usage such as wearable devices on human body, however, the device could suffer
31 from mechanical damage due to periodical external mechanical motion, resulting in poor
32 performance. Fortunately, based on the cooperative self-healing abilities of triboelectric layer
33 and electrode, the whole device could achieve entire self-heal to maintain not only mechanical
34 but also electrical performances. Accordingly, the electric output of the prepared TENGs were
35 systematically investigated under different healing time, temperature, and NIR irradiation.
36 The safety and lifespan of the device were further guaranteed through diverse healing
37 approaches. **Figure 4a** and **b** present the V_{oc} and I_{sc} of the original, broken and self-healed IU-
38 TENG after three different healing times from 3 to 6 h and then to 9 h at 34 °C which is close
39 to the surface temperature of human skin. When the IU-TENG was cut from the middle, both
40 of the V_{oc} and I_{sc} drop by almost half to 46 V and 4.8 μ A, respectively, attributed to the
41 decrease of effective contact areas. Then the broken surfaces were brought into full contact.
42 From Figure 4c, it was found that the time-dependent healing process was completed after 9 h
43
44
45
46
47
48
49
50
51
52
53
54
55
56
57
58
59
60
61
62
63
64
65

1
2
3
4
5
6
7
8
9
10
11
12
13
14
15
16
17
18
19
20
21
22
23
24
25
26
27
28
29
30
31
32
33
34
35
36
37
38
39
40
41
42
43
44
45
46
47
48
49
50
51
52
53
54
55
56
57
58
59
60
61
62
63
64
65

at 34 °C. The V_{oc} and I_{sc} of self-healed IU-TENG at different temperatures (15, 25, 34, 45 and 55 °C) for 9 h are exhibited in Figure 4d and e. The healing process was also temperature-dependent, as shown in Figure 4f. Above 34 °C, the whole recovery time of device might last about 9 h. While the temperature was lower than 34 °C, the repair time of device could be elongated due to relatively low molecular activity. Moreover, the IU-TENG could perform fast self-repair under assistance of NIR irradiation for 30 min (Figure 4g and h). The repeated self-healing feature of IU-TENG was further investigated as shown in Figure 4i. After broken and repaired for 6 times, the V_{oc} and I_{sc} of self-healed IU-TENG remained almost same values with original device. It was worth noting that under NIR irradiation, the temperature of MWCNTs-UPy/IU-PAM rapidly rose to 120 °C (Figure 2d), indicating that the IU-TENG exhibited stable output performance over a wide temperature range. Those results presented that, under different temperature or NIR irradiation, the electrical performance of IU-TENG device could restore to its original state.

34
35
36
37
38
39
40
41
42
43
44
45
46
47
48
49
50
51
52
53
54
55
56
57
58
59
60
61
62
63
64
65

Benefiting from the excellent self-healing properties of IU-TENG, the as-prepared device was endowed with shape-tailorable capability, which extend TENGs to satisfy different applications with various shapes. In our previous work, shape-tailorable TENGs have been fabricated using healable polymer, magnetic balls and cubes.^[36] The shape-tailorability of TENG device was limited by the rigid magnetic components. By utilization of flexible self-healing and conductive materials, we further enhance the shape-tailorability of TENG which could be tailored into arbitrary shapes. As shown in **Figure 5a**, the original IU-TENG was cut into different shapes including arc, square, and triangle shape which were utilized to assemble TENG in different shapes (shape 1-3). The V_{oc} and I_{sc} of the original, after cutting, and shape 1 to 3 after healing were presented in Figure 5b. After cutting, contact areas of TENG decreased, leading to the decrement of the V_{oc} and I_{sc} . Once the pieces were assembled into an intact shape for self-healing, the V_{oc} and I_{sc} recover to about 95 V and 9.4 μ A, respectively.

1 All of the re-shaped IU-TENGs exhibited excellent output electrical performances, which
2 were same as that of original device. These excellent results demonstrated the outstanding
3 shape-tailorability of IU-TENG.
4
5
6
7
8

9 **2.6. Self-powered Sensor**

10
11 Followed by the above systematical investigations of output performance, self-healing
12 capability, and tailorability, IU-TENG could be utilized as self-powered sensor to detect
13 human motion. Structure of TENG device based on IU-TENG with 40 mm × 20 mm is
14 designed and schematically depicted in **Figure 6a**. The bottom layer (IU-PDMS) is an
15 insulator to separate human body from the electrode. The middle electrode (MWCNTs-
16 UPy/IU-PAM) is tightly attached to the bottom one through self-bonding, driven by the
17 reversible exchange of imine bonds and UPy moieties. Additionally, the middle electrode and
18 top layer (IU-PDMS) served as electrification layers, which were separated by two small
19 spacers (IU-PDMS) to realize the contact-separation motions under the external force. The as-
20 fabricated flexible TENG device could be used as a self-powered finger-joint motion sensor,
21 which could be properly attached to the finger in a straight state (Figure 6b) and subjected to
22 bend (Figure 6c). With the bending angle periodically changing from 30° to 60° and then to
23 90°, the output V_{oc} was 0.6 V, 1.4 V, and 2.7 V, respectively (Figure 6d). As the bending
24 angle increased, the contact area of two triboelectric layers was enlarged, leading to rising the
25 V_{oc} of the TENG sensor simultaneously. Therefore, the change of bending angle in the finger-
26 joint motion can be monitored via the change of open-circuit voltage. In addition, the gap
27 between the triboelectric layers had a significant influence on the output performance. The
28 potential distribution of two triboelectrically charged materials under open-circuit condition
29 are simulated by COMSOL (Figure 6f). From the simulation results, it was obviously
30 observed that the open-circuit voltage was proportional to the gap between triboelectric layers,
31 indicating the detection signal could be enhanced through enlarging the gap (Figure 6g).
32
33
34
35
36
37
38
39
40
41
42
43
44
45
46
47
48
49
50
51
52
53
54
55
56
57
58
59
60
61
62
63
64
65

1
2 During device operation, the as-prepared self-powered sensor might be damaged or destroyed
3
4 by frequent bending and friction. Providentially, the broken device on the finger could be
5
6 timely self-healed based on thermal effect of IR radiation from skin. In addition, if the device
7
8 was taken off from body, NIR could be utilized to facilitate fast self-healing processes.
9
10 Multiple repairing methods can ensure and enhance reliability and safety of device. Most of
11
12 human body heat is dissipated as IR radiation, and the reported IR emittance of skin is 0.98.^[47]
13
14 As a result, human skin can be considered as natural IR emitter. At the skin temperature of
15
16 34 °C, IR radiation from human body is mainly in the range of 8-14 μm with the peak
17
18 emission at the wavelength of 9.5 μm.^[47-48] Under IR light ranging from 0.5 to 3 μm, the
19
20 temperature of MWCNTs-UPy/IU-PAM rose rapidly, resulting from the good photothermal
21
22 effect of MWCNTs-UPy (**Figure 7a-c**). Moreover, the measured IR emittance of MWCNTs-
23
24 UPy/IU-PAM was 0.91 in the range of 1.5 to 21 μm, further indicating the as-prepared TENG
25
26 device could efficiently absorb the IR radiation. As the TENG device was attached to finger,
27
28 the temperature of materials increased under the IR radiation from human body, which could
29
30 promote self-healing (**Figure 6a-c**). The device was scratched, and assembled together in full
31
32 contact, and then put on skin. After complete healing, the device could still be subjected to
33
34 bend from 30° to 90°, with the V_{oc} increasing from 0.6 V to 2.6 V, which was almost
35
36 consistent with that of the original one (**Figure 6e**). The results suggested that the as-
37
38 fabricated TENG device served as a self-powered sensor exhibited excellent self-healing
39
40 performance under the IR radiation from human body.
41
42
43
44
45
46
47
48
49
50
51
52

53 **3. Conclusion**

54
55 In summary, entirely self-healing, flexible and tailorable TENGs with robust interface
56
57 bonding have been developed for potential applications in self-powered sensors. Attributed to
58
59 both electrode and electrification layer containing the dynamic imine bonds and UPy moieties,
60
61
62
63
64
65

1 the different layers were seamlessly integrated into a single system through the exchange of
2 dynamic bonds at interfaces, ensuring the TENG device mechanically robust and electrically
3
4 stable. The UPy units were intentionally incorporated into imine-based elastomers to improve
5
6 the mechanics performance and synergistically motivate self-healing. By modifying the
7
8 MWCNTs with UPy motif, a good compatibility between nanofillers and polymer segments
9
10 was achieved to facilitate the reconfiguration of conductive networks during repair.
11
12 Meanwhile, our designed and synthesized materials (IU-PDMS and MWCNTs-UPy/IU-PAM)
13
14 and the assembled IU-TENG device exhibited intrinsically unique self-healing feature driven
15
16 by the reversible bonds based molecular interconnects, with mechanical and electrical
17
18 properties well recovered. Furthermore, the self-healing TENG could be easily tailored and
19
20 implemented on self-powered devices to detect human motions, with IR thermal radiation
21
22 from human skin effectively promoting self-healing to realize timely recovery after damage.
23
24 This can be the foundation of integration design of self-healing and self-powered soft devices
25
26 for reliability, safety and environmental sustainability.
27
28
29
30
31
32
33
34
35

36 **4. Experimental Section**

37
38 *Materials:* 2-Amino-4-hydroxy-6-methylpyrimidine (MIC, 98.0%), hexamethylene
39
40 diisocyanate (HDI, 99.0%), poly(propylene glycol)bis(2-aminopropyl ether) (PEA, $M_n = 2000$)
41
42 were purchased from Aladdin. Bis(3-aminopropyl) terminated poly(dimethylsiloxane) (H_2N-
43
44 PDMS-NH₂, $M_n = 5000-7000$) were purchased from Gelest. Amino-functionalized multi-
45
46 walled carbon nanotubes (MWCNTs-NH₂, average diameter of 8-15 nm, length of 50 μ m)
47
48 were purchased from Nanjing XFNANO Materials Tech. Co. Ltd. 1, 1, 1-tris[(4-
49
50 formylphenoxy)methyl]ethane (FPME) were prepared via previously reported procedures.^[32]
51
52
53 All reagents were utilized as supplied without further purification.
54
55
56
57
58
59
60

61 *Synthesis of UPy-NCO:* The synthesis was carried out according to the reported procedures,^[49]
62
63
64
65

1 as shown in Figure S1 (Supporting Information). 2-Amino-4-hydroxy-6-methylpyrimidine
2 (1.25g, 0.01 mol) and hexamethylene diisocyanate (11.44 mL, 0.068mol) were mixed in a
3 flask equipped with a reflux condenser with stirring at 100 °C under nitrogen atmosphere for
4 24 h. After cooling to room temperature, pentane was poured into the mixture. The precipitate
5 was collected and dried at 50 °C in vacuum for overnight.
6
7
8
9
10

11
12
13
14 *Preparation of MWCNTs-UPy:* As shown in Figure S3 (Supporting Information), to a solution
15 of UPy-NCO (0.4 g) in 50 mL of anhydrous N, N-dimethylformamide (DMF), MWCNTs-
16 NH₂ (0.4 g) was added and ultra-sonicated for 30 min. The mixture was kept at 80 °C to
17 continue the reaction under nitrogen atmosphere for 24 h with vigorously mechanical stirring.
18
19 The MWCNTs-UPy product was separated from the suspension and washed with DMF and
20 dichloromethane, and dried at 60 °C under vacuum oven for 24 h.
21
22
23
24
25
26
27
28
29
30

31
32 *Preparation of IU-PAM:* For IU-PAM-2 sample preparation, PEA 2000 (2.7 g, 1.35 mmol)
33 and UPy-NCO (0.135 g, 0.45 mmol) were dissolved in 8 mL of DMF. The mixture was
34 heated at 80 °C for 6 h. After cooling to room temperature, FPME (0.342g, 0.75 mmol) and
35 glacial acetic acid (AcOH, 25 µL) were added with stirring for 12 h. After reaction, the
36 solvent was evaporated and dried in an oven overnight. Then the product (3 g) was dissolved
37 in 15 mL of chloroform (CHCl₃). The solution was poured into a Teflon dish and allowed to
38 slowly evaporate at room temperature overnight. Finally, the resulting film was dried in a
39 vacuum oven at 60 °C for 24 h. The same procedure was used to prepare films based on other
40 IU-PAMs (Table S1).
41
42
43
44
45
46
47
48
49
50
51
52
53
54
55

56 *Preparation of MWCNTs-UPy/IU-PAM Nanocomposite:* IU-PAM-2 (3 g) was dissolved in 15
57 mL of CHCl₃, followed by adding the synthesized MWCNTs-UPy (0.158 g, 5 wt%). The
58 mixture was ultra-sonicated for 30 min, and transferred into a Teflon mould, which was
59
60
61
62
63
64
65

1 allowed to slowly evaporate solvent at room temperature. The obtained film was dried in an
2 oven for 24 h.
3

4
5
6
7 *Preparation of IU-PDMS:* UPy-NCO (0.06 g, 0.2 mmol) was added to the solution of H₂N-
8 PDMS-NH₂ (3 g, 0.6 mmol) in 15 mL of CHCl₃, and the mixture was heated at 60 °C under
9 reflux for 6 h. After the solution was cooled to room temperature, FPME (0.152g, 0.333 mmol)
10 was added and stirred overnight. The solution was casted on a Teflon mold and dried at room
11 temperature for 24 h followed by drying at 60 °C for 24 h in a vacuum oven.
12
13
14
15
16
17
18
19
20

21
22 *Fabrication of IU-TENG:* The prepared MWCNTs-UPy/IU-PAM nanocomposite and IU-
23 PDMS films (0.5 mm thick) were cut into squares (40 mm × 40 mm) with a razor,
24 respectively. The self-healing TENG device was fabricated by sandwiching the MWCNTs-
25 UPy/IU-PAM nanocomposite layer between the two IU-PDMS layers with a copper tape
26 attached to the nanocomposite for the convenience of measurement.
27
28
29
30
31
32
33
34
35

36
37 *Fabrication of Self-Healing TENG Sensor:* The prepared MWCNTs-UPy/IU-PAM
38 nanocomposite and IU-PDMS films (0.5 mm thick) were cut into rectangles (40 mm × 20 mm)
39 with a razor, respectively. A piece of MWCNTs-UPy/IU-PAM nanocomposite film was
40 placed on top of the IU-PDMS film. Then another layer of IU-PDMS with the spacer (2 mm
41 thick) was attached to the MWCNTs-UPy/IU-PAM through self-bonding.
42
43
44
45
46
47
48
49
50

51
52 *Characterization:* NMR analyses were conducted on a Bruker Avance 400 instrument. FTIR
53 tests were performed on a Nicolet iS10 IR spectrometer (Thermo Scientific, USA). The
54 mechanical tensile tests were performed using an Instron 3342 universal tester with a
55 stretching speed of 20 mm min⁻¹ according to ISO37-4. The healing efficiency was defined as
56 the ratio of elongation at break of healed specimens to that of original specimens. DSC was
57
58
59
60
61
62
63
64
65

1 performed using a Mettler Toledo DSC 1 instrument with the heating rate of 10 °C min⁻¹.
2 TGA analyses were recorded using a STA, 449C Jupiter instrument under an argon
3 atmosphere with a heating rate of 10 K min⁻¹. TEM (FEI Talos F200X) was operated at an
4 accelerating voltage of 200 kV. Resistance measurements were conducted on Keithley 2450
5 source meter. The output voltage was measured by an oscilloscope (LeCroy WaveSurfer 62Xs
6 600MHz 2.5 GS/s). The output current was characterized by a low noise current amplifier
7 (Stanford Research Systems, SR570). The charge transfer was measured using an
8 electrometer (Keithley 6514). Infrared thermal images were recorded by a Fluke Ti300
9 infrared imager. IR emittance was performed using an AZUP ET100 infrared emissivity meter
10 in the range of 1.5-21 μm.
11
12
13
14
15
16
17
18
19
20
21
22
23
24
25

26 **Supporting Information**

27 Supporting Information to this article is available from the Wiley Online Library or from the
28 author.
29
30
31
32
33
34
35

36 **Acknowledgements**

37 X. D. and L.-B. H. contributed equally to this work. The research was financially supported
38 by the National Natural Science Foundation of China through grants (Grand No.21875190
39 and 51973119), Shaanxi Natural Science Funds for Distinguished Young Scholars (2018JC-
40 008), the Natural Science Foundation of Guang Dong Province (Grand No.2018A0303130060
41 and 2019A1515011566), and the Science and Technology Innovation Commission of
42 Shenzhen City (JCYJ20170818101245583).
43
44
45
46
47
48
49
50
51
52
53
54
55

56 Received: ((will be filled in by the editorial staff))

57 Revised: ((will be filled in by the editorial staff))

58 Published online: ((will be filled in by the editorial staff))
59
60
61
62
63
64
65

References

- 1
2 [1] Z. L. Wang, *Adv. Mater.* **2012**, *24*, 280.
3
4 [2] H. Chen, Y. Song, X. Cheng, H. Zhang, *Nano Energy* **2019**, *56*, 252.
5
6 [3] S. S. Kwak, H.-J. Yoon, S.-W. Kim, *Adv. Funct. Mater.* **2019**, *29*, 1804533.
7
8 [4] S. Park, S. W. Heo, W. Lee, D. Inoue, Z. Jiang, K. Yu, H. Jinno, D. Hashizume, M.
9
10 Sekino, T. Yokota, K. Fukuda, K. Tajima, T. Someya, *Nature* **2018**, *561*, 516.
11
12 [5] F. R. Fan, W. Tang, Z. L. Wang, *Adv. Mater.* **2016**, *28*, 4283.
13
14 [6] Z. L. Wang, J. Chen, L. Lin, *Energy Environ. Sci.* **2015**, *8*, 2250.
15
16 [7] M. Xu, T. Zhao, C. Wang, S. L. Zhang, Z. Li, X. Pan, Z. L. Wang, *ACS Nano* **2019**, *13*,
17
18 1932.
19
20 [8] G. Yao, D. Jiang, J. Li, L. Kang, S. Chen, Y. Long, Y. Wang, P. Huang, Y. Lin, W.
21
22 Cai, X. Wang, *ACS Nano* **2019**, *13*, 12345.
23
24 [9] X. Li, G. Xu, X. Xia, J. Fu, L. Huang, Y. Zi, *Nano Energy* **2019**, *56*, 40.
25
26 [10] Y. Zi, J. Wang, S. Wang, S. Li, Z. Wen, H. Guo, Z. L. Wang, *Nat. Commun.* **2016**, *7*,
27
28 10987.
29
30 [11] X.-S. Zhang, M. Han, B. Kim, J.-F. Bao, J. Brugger, H. Zhang, *Nano Energy* **2018**, *47*,
31
32 410.
33
34 [12] G. Liu, J. Chen, Q. Tang, L. Feng, H. Yang, J. Li, Y. Xi, X. Wang, C. Hu, *Adv. Energy*
35
36 *Mater.* **2018**, *8*, 1703086.
37
38 [13] L.-B. Huang, W. Xu, G. Bai, M.-C. Wong, Z. Yang, J. Hao, *Nano Energy* **2016**, *30*, 36.
39
40 [14] J. H. Lee, R. Hinchet, S. K. Kim, S. Kim, S.-W. Kim, *Energy Environ. Sci.* **2015**, *8*,
41
42 3605.
43
44 [15] X. Cao, M. Zhang, J. Huang, T. Jiang, J. Zou, N. Wang, Z. L. Wang, *Adv. Mater.* **2018**,
45
46 *30*, 1704077.
47
48 [16] L.-B. Huang, G. Bai, M.-C. Wong, Z. Yang, W. Xu, J. Hao, *Adv. Mater.* **2016**, *28*,
49
50 2744.
51
52
53
54
55
56
57
58
59
60
61
62
63
64
65

- 1 [17] T. P. Huynh, P. Sonar, H. Haick, *Adv. Mater.* **2017**, *29*, 1604973.
- 2 [18] D. Chen, D. Wang, Y. Yang, Q. Huang, S. Zhu, Z. Zheng, *Adv. Energy Mater.* **2017**, *7*,
- 3 1700890.
- 4
- 5
- 6 [19] M. D. Bartlett, M. D. Dickey, C. Majidi, *NPG Asia Mater.* **2019**, *11*, 1.
- 7
- 8 [20] S. Y. An, D. Arunbabu, S. M. Noh, Y. K. Song, J. K. Oh, *Chem. Commun.* **2015**, *51*,
- 9 13058.
- 10
- 11
- 12 [21] J. Kang, J. B. H. Tok, Z. Bao, *Nat. Electron.* **2019**, *2*, 144.
- 13
- 14 [22] L. M. Zhang, Y. He, S. Cheng, H. Sheng, K. Dai, W. J. Zheng, M. X. Wang, Z. S.
- 15 Chen, Y. M. Chen, Z. Suo, *Small* **2019**, *15*, 1804651.
- 16
- 17 [23] Y. Yang, M. W. Urban, *Adv. Mater. Interfaces* **2018**, *5*, 1800384.
- 18
- 19 [24] X. Yan, F. Wang, B. Zheng, F. Huang, *Chem. Soc. Rev.* **2012**, *41*, 6042.
- 20
- 21 [25] R. J. Wojtecki, M. A. Meador, S. J. Rowan, *Nat. Mater.* **2011**, *10*, 14.
- 22
- 23 [26] W. Zou, J. Dong, Y. Luo, Q. Zhao, T. Xie, *Adv. Mater.* **2017**, *29*, 1606100.
- 24
- 25 [27] P. Chakma, D. Konkolewicz, *Angew. Chem. Int. Ed.* **2019**, *58*, 9682.
- 26
- 27 [28] X. Wu, J. Wang, J. Huang, S. Yang, *ACS Appl. Mater. Interfaces* **2019**, *11*, 7387.
- 28
- 29 [29] M. Liu, P. Liu, G. Lu, Z. Xu, X. Yao, *Angew. Chem. Int. Ed.* **2018**, *57*, 11242.
- 30
- 31 [30] J. Chen, Q. Peng, T. Thundat, H. Zeng, *Chem. Mater.* **2019**, *31*, 4553.
- 32
- 33 [31] C.-H. Li, C. Wang, C. Keplinger, J.-L. Zuo, L. Jin, Y. Sun, P. Zheng, Y. Cao, F. Lissel,
- 34 C. Linder, X.-Z. You, Z. Bao, *Nat. Chem.* **2016**, *8*, 618.
- 35
- 36 [32] X. Dai, Y. Du, J. Yang, D. Wang, J. Gu, Y. Li, S. Wang, B. B. Xu, J. Kong, *Compos.*
- 37 *Sci. Technol.* **2019**, *174*, 27.
- 38
- 39 [33] Z. Zou, C. Zhu, Y. Li, X. Lei, W. Zhang, J. Xiao, *Sci. Adv.* **2018**, *4*, eaaq0508.
- 40
- 41 [34] Z. Wei, D. M. Lewis, Y. Xu, S. Gerecht, *Adv. Healthc. Mater.* **2017**, *6*, 1700523.
- 42
- 43 [35] A. Rekondo, R. Martin, A. Ruiz de Luzuriaga, G. Cabanero, H. J. Grande, I. Odriozola,
- 44 *Mater. Horiz.* **2014**, *1*, 237.
- 45
- 46 [36] W. Xu, L.-B. Huang, J. Hao, *Nano Energy* **2017**, *40*, 399.
- 47
- 48
- 49
- 50
- 51
- 52
- 53
- 54
- 55
- 56
- 57
- 58
- 59
- 60
- 61
- 62
- 63
- 64
- 65

- 1
2
3
4
5
6
7
8
9
10
11
12
13
14
15
16
17
18
19
20
21
22
23
24
25
26
27
28
29
30
31
32
33
34
35
36
37
38
39
40
41
42
43
44
45
46
47
48
49
50
51
52
53
54
55
56
57
58
59
60
61
62
63
64
65
- [37] J. Sun, X. Pu, M. Liu, A. Yu, C. Du, J. Zhai, W. Hu, Z. L. Wang, *ACS Nano* **2018**, *12*, 6147.
- [38] Q. Guan, Y. Dai, Y. Yang, X. Bi, Z. Wen, Y. Pan, *Nano Energy* **2018**, *51*, 333.
- [39] Y.-C. Lai, H.-M. Wu, H.-C. Lin, C.-L. Chang, H.-H. Chou, Y.-C. Hsiao, Y.-C. Wu, *Adv. Funct. Mater.* **2019**, *29*, 1904626.
- [40] J. A. Neal, D. Mozhdghi, Z. Guan, *J. Am. Chem. Soc.* **2015**, *137*, 4846.
- [41] H. Zhang, Y. Wu, J. Yang, D. Wang, P. Yu, C. T. Lai, A.-C. Shi, J. Wang, S. Cui, J. Xiang, N. Zhao, J. Xu, *Adv. Mater.* **2019**, *31*, 1904029.
- [42] Y. Song, Y. Liu, T. Qi, G. L. Li, *Angew. Chem. Int. Ed.* **2018**, *57*, 13838.
- [43] F. Song, Z. Li, P. Jia, M. Zhang, C. Bo, G. Feng, L. Hu, Y. Zhou, *J. Mater. Chem. A* **2019**, *7*, 13400.
- [44] T. T. T. Myllymäki, L. Lemetti, Nonappa, O. Ikkala, *ACS Macro Letters* **2017**, *6*, 210.
- [45] C.-R. Chen, H. Qin, H.-P. Cong, S.-H. Yu, *Adv. Mater.* **2019**, *31*, 1900573.
- [46] W. Pu, D. Fu, Z. Wang, X. Gan, X. Lu, L. Yang, H. Xia, *Adv. Sci.* **2018**, *5*, 1800101.
- [47] L. Cai, A. Y. Song, W. Li, P.-C. Hsu, D. Lin, P. B. Catrysse, Y. Liu, Y. Peng, J. Chen, H. Wang, J. Xu, A. Yang, S. Fan, Y. Cui, *Adv. Mater.* **2018**, *30*, 1802152.
- [48] A. Hazarika, B. K. Deka, C. Jeong, Y.-B. Park, H. W. Park, *Adv. Funct. Mater.* **2019**, *29*, 1903144.
- [49] B. J. B. Folmer, R. P. Sijbesma, R. M. Versteegen, J. A. J. van der Rijt, E. W. Meijer, *Adv. Mater.* **2000**, *12*, 874.

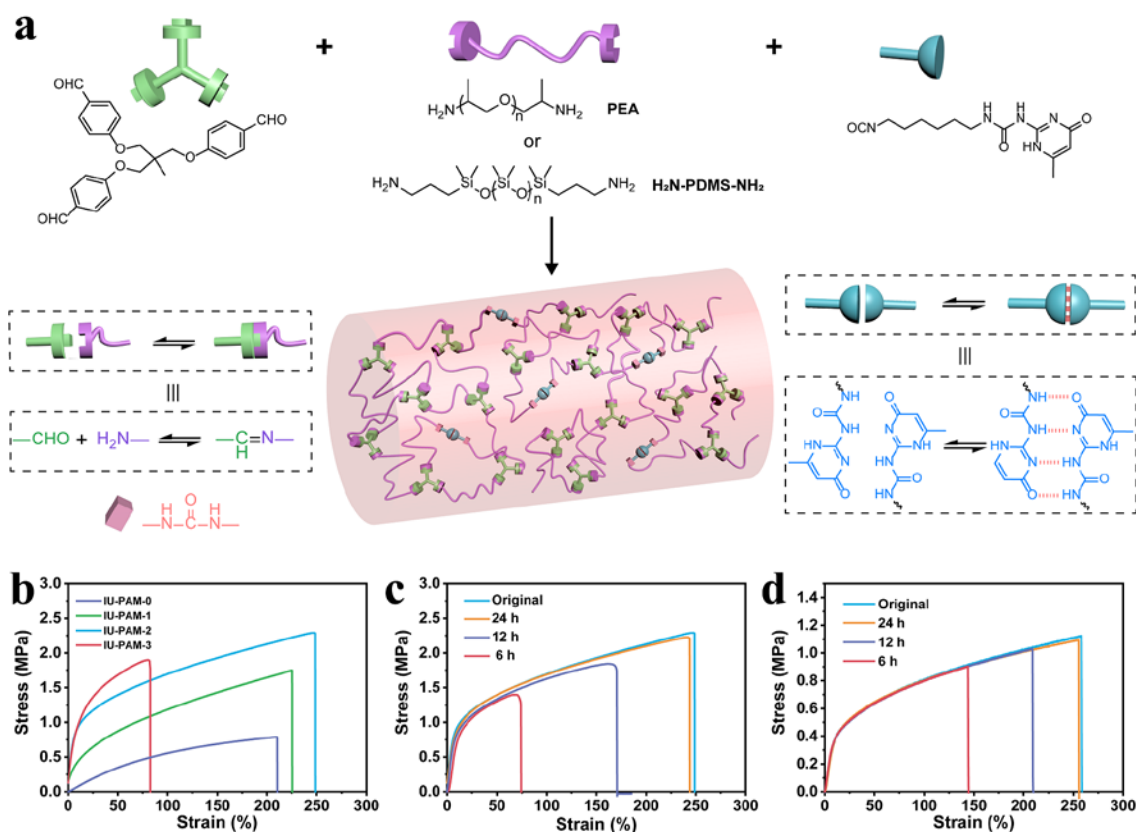


Figure 1. Schematic illustration of the design of self-healing polymeric materials (IU-PAM and IU-PDMS) and mechanical characterization. (a) Chemical structures of IU-PAM and IU-PDMS cross-linked by dynamic imine bonds and UPy. (b) Stress-strain curves of IU-PAM-0-3 with varying amounts of UPy cross-links to tune mechanical properties. Stress-strain curves of the original and self-healed (c) IU-PAM-2 and (d) IU-PDMS specimens after three different healing times from 6 to 12 h and then to 24 h at room temperature.

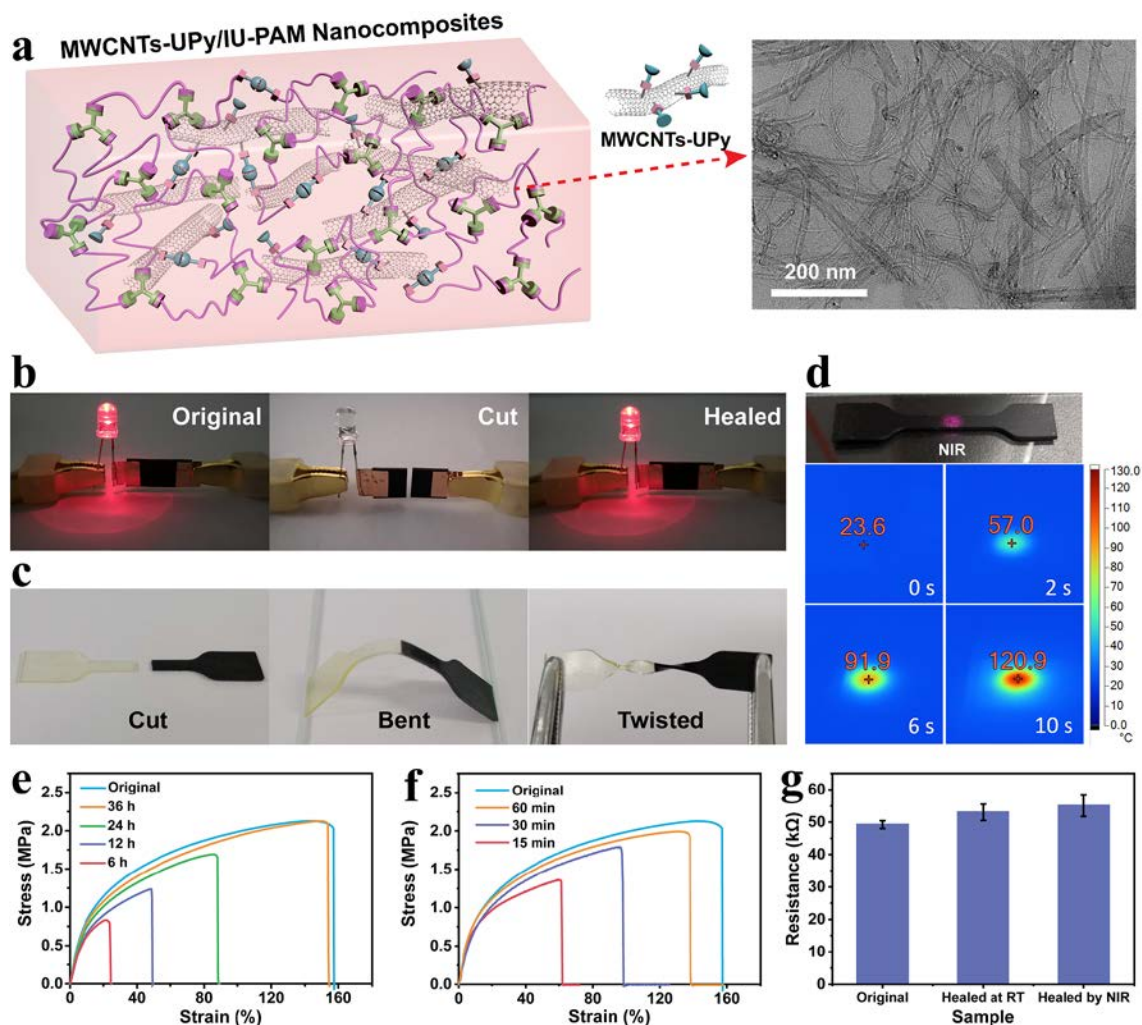


Figure 2. Characterization and performance of the self-healing nanocomposite. (a) Illustration of the structure for MWCNTs-UPy/IU-PAM nanocomposite with a TEM image. (b) Optical images of MWCNTs-UPy/IU-PAM nanocomposite (the original, after cutting and after healing) in a circuit with an LED bulb. (c) Self-healing enabled welding of cut dumbbell between the IU-PDMS and MWCNTs-UPy/IU-PAM. (d) Time-lapse FLIR images of MWCNTs-UPy/IU-PAM nanocomposite. Stress–strain curves of the original and self-healed MWCNTs-UPy/IU-PAM after different healing times (e) at room temperature and (f) under NIR laser irradiation. (g) Electrical resistance of the original and self-healed MWCNTs-UPy/IU-PAM nanocomposite.

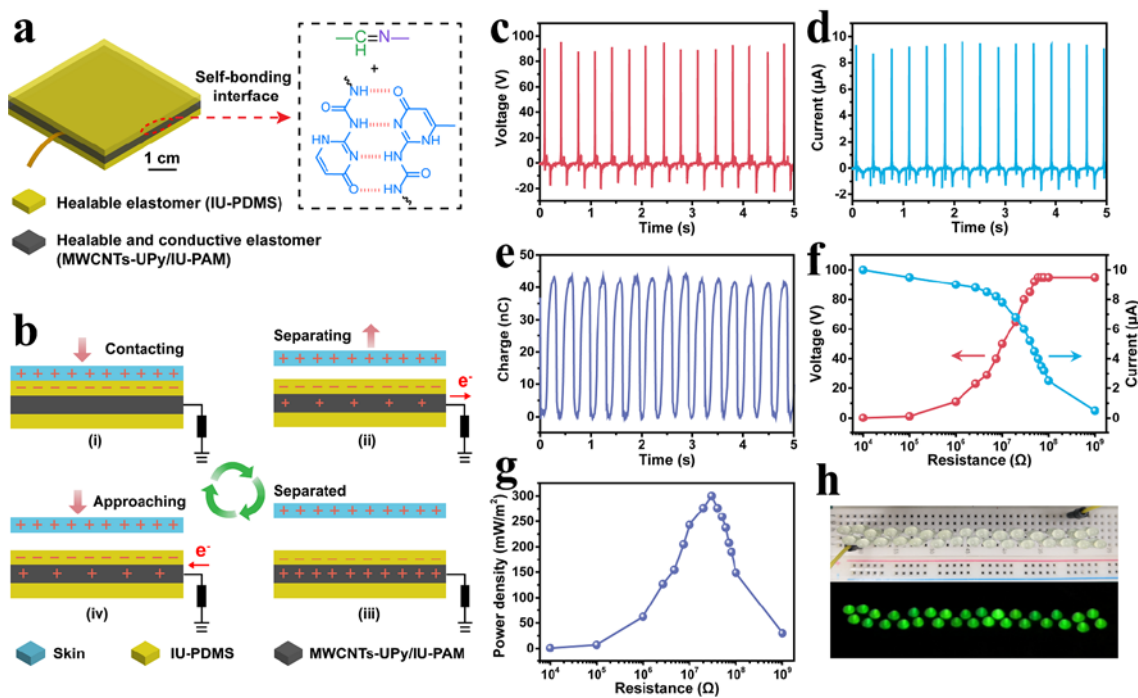


Figure 3. Fabrication and Electrical output performance of the IU-TENG. (a) Diagram of self-healing IU-TENG. (b) Schematic illustration of the working mechanism of the IU-TENG device in single-electrode mode. (c) Open-circuit voltage, (d) short-circuit current, and (e) transferred charge of IU-TENG under contact and separation with a frequency of 3 Hz. (f) Output voltage and current versus resistance. (g) Variation of power density with external resistance. (h) Photograph of thirty green LEDs connected in series driven by the IU-TENG.

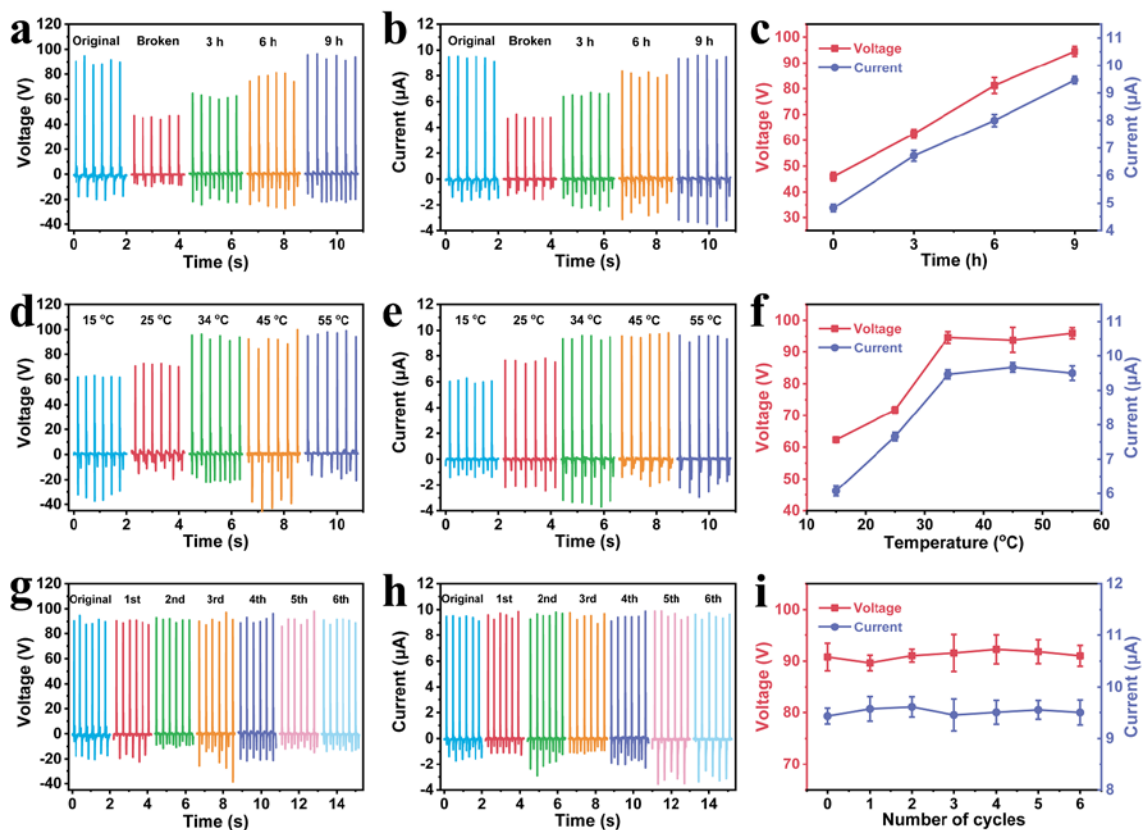


Figure 4. Output characteristics of IU-TENG under varying healing conditions. (a) Open-circuit voltage and (b) short-circuit current of the original, broken and self-healed IU-TENG after three different healing times from 3 to 6 h and then to 9 h at 34 °C. (c) Voltage and current change of IU-TENG after different healing times at 34 °C. (d) Open-circuit voltage and (e) short-circuit current of self-healed IU-TENG at different temperatures (15, 25, 34, 45 and 55 °C) for 9 h. (f) Voltage and current change of IU-TENG at different healing temperatures for 9 h. (g) Open-circuit voltage and (h) short-circuit of the original and self-healed IU-TENG after one to four cycles under NIR irradiation. (i) Voltage and current change of IU-TENG after healing under NIR irradiation for several cycles (0 represent the original).

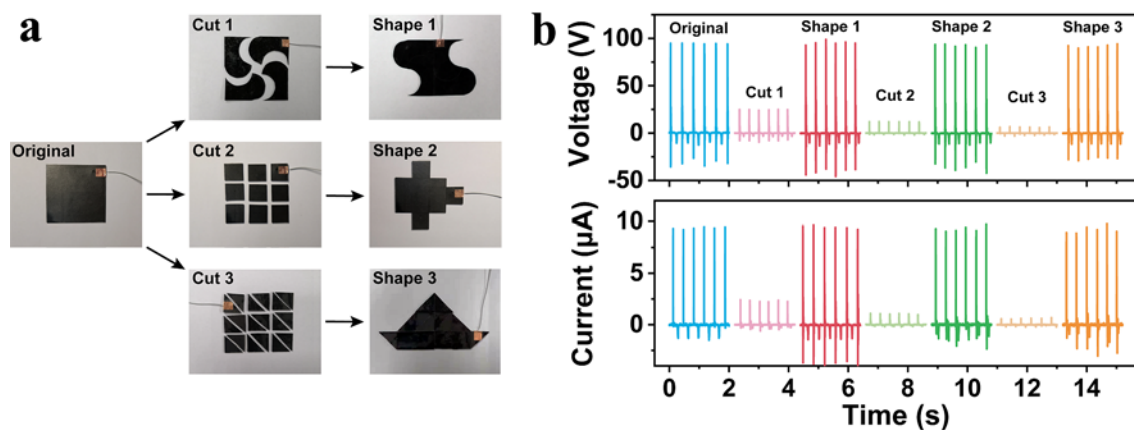


Figure 5. Shape-tailorable performance of IU-TENG. (a) Optical images of the tailorable process for the IU-TENG (the original, after cutting into 4, 9, and 18 pieces, and shape 1 to 3 after healing). (b) Open-circuit voltage and short-circuit current of the original, cut and re-shaped IU-TENG.

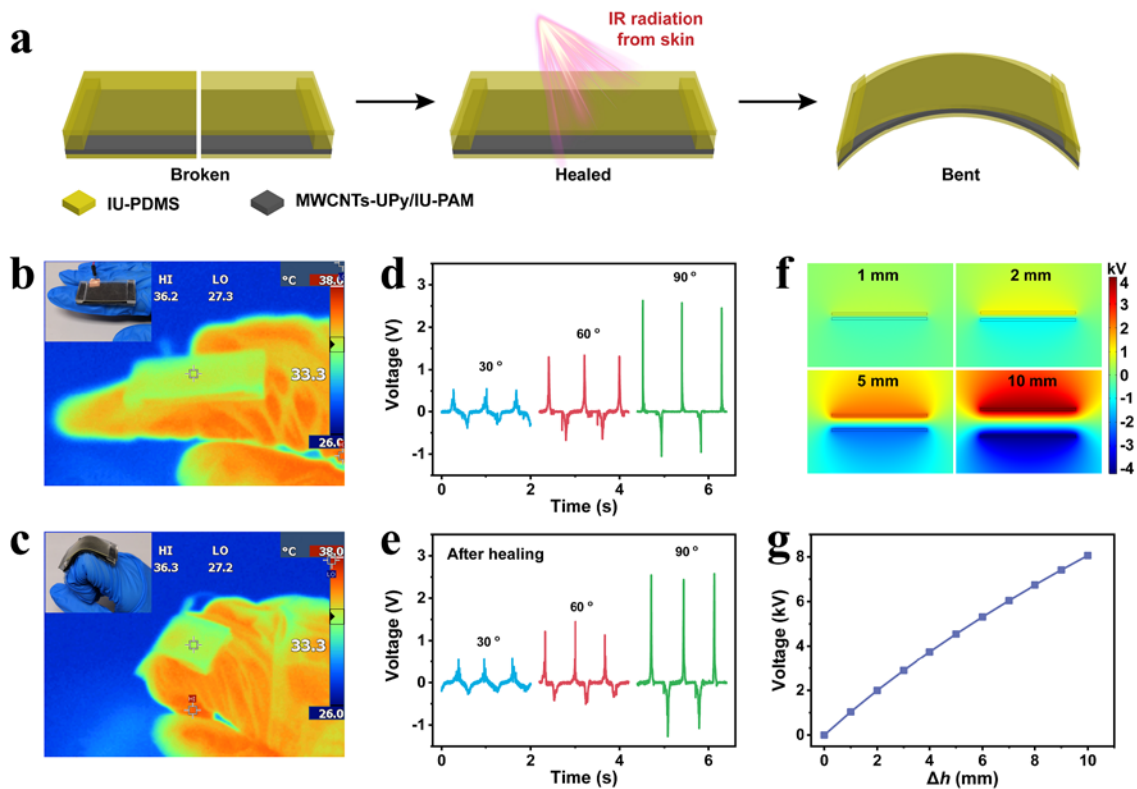


Figure 6. Demonstration of the self-healable TENG for human motion detection. (a) Schematic diagrams of the self-healing TENG via IR radiation from skin. Thermal images with inset optical images of (b) the original and (c) bent TENG on the finger. Open-circuit voltage responses when bending the finger joint at different angles (30°, 60° and 120°) of (d) the original and (e) self-healed TENG. (f, g) Numerical calculation of the potential distribution of the TENG at varying gap between IU-PDMS and MWCNTs-UPy/IU-PAM nanocomposite by using COMSOL software.

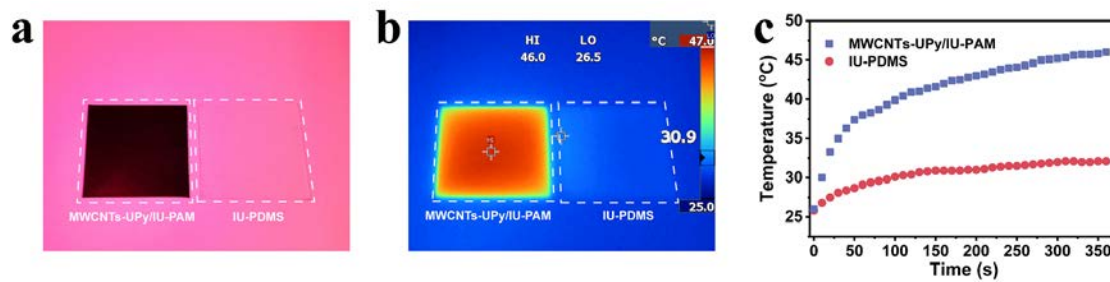


Figure 7. IR absorption characteristics of MWCNTs-UPy/IU-PAM and IU-PDMS. (a) Optical image and (b) thermal image of MWCNTs-UPy/IU-PAM (left) and IU-PDMS (right) under IR lamp. (c) Temperature rise of samples under IR irradiation for 360 s.

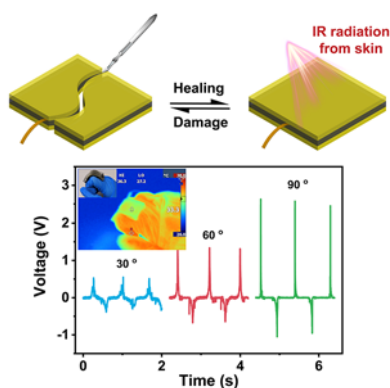
An entirely self-healing, flexible and tailorable TENG as a self-powered sensor to monitor human motion is designed. Human skin serving as natural infrared emitter could provide a favorable condition for the device to realize real-time self-healing, based on thermal effect of IR radiation. The proposed strategy is general, contributing to future sustainable energy and wearable devices.

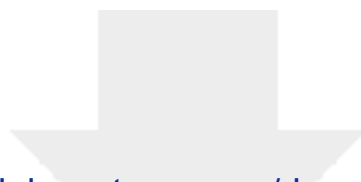
Keywords: triboelectric nanogenerators, self-powered sensors, self-healing, infrared radiation, reversible bonds.

Xingyi Dai, Long-Biao Huang, Yuzhang Du, Jiancheng Han, Qiuqun Zheng, Jie Kong* and Jianhua Hao**

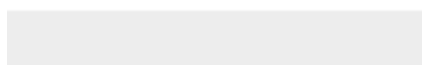
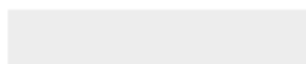
Self-Healing, Flexible, and Tailorable Triboelectric Nanogenerators for Self-Powered Sensors based on Thermal Effect of Infrared Radiation

ToC Figure:





Click here to access/download
Supporting Information
Supporting Information for AFM.pdf





Click here to access/download
Production Data
Manuscript for production.pdf

